Ludden, J.N., Plank, T., and Escutia, C. (Eds.)
Proceedings of the Ocean Drilling Program, Scientific Results Volume 185

11. Data Report: Measurement of Mass Transfer Properties with Subducted Oceanic Plate[1]

Tetsuro Hirono[2]

INTRODUCTION

The subduction of oceanic plates regulates crustal growth, influences arc volcanism, and refertilizes the mantle. Continental growth occurs by subduction of crustal material (seawater components, marine sediments, and basaltic crust). The geochemical and physical evolution of the Earth's crust depends, in large part, on the fate of subducted material at convergent margins (Armstrong, 1968; Karig and Kay, 1981). The crustal material on the downgoing plate is recycled to various levels in the subduction zone. The recycling process that takes place in the "Subduction Factory" is difficult to observe directly but is clearly illuminated using chemical tracers. Von Huene and Scholl (1991) and Plank and Langmuir (1993) preliminarily calculated a large flux of subducted materials. By mass balancing the chemical tracers and measuring the fractionations that occur between them, the Subduction Factory work and the effect on the Earth's evolution can be estimated. In order to elucidate this mass balance, Ocean Drilling Program Leg 185 drilled two deepwater shales into the oceanic crust situated in the Mariana-Izu Trenches and recovered core samples of incoming oceanic crust.

The calculations of mass circulation in the subduction zone, however, did not take into account the mass transfer properties within subducted oceanic crust, although the dewatering fluid and diffused ions may play an important role in various activities such as seismogeneity, serpentine diapiring, and arc volcanism. Thus, this paper focuses on the quantitative measurements of the physical and mass transfer properties of subducted oceanic crust.

[1]Hirono, T., 2003. Data report: Measurement of mass transfer properties with subducted oceanic plate. *In* Ludden, J.N., Plank, T., and Escutia, C. (Eds.), *Proc. ODP, Sci. Results,* 185, 1–14 [Online]. Available from World Wide Web: <http://www-odp.tamu.edu/publications/185_SR/VOLUME/CHAPTERS/002.PDF>. [Cited YYYY-MM-DD]
[2]Deep Sea Research Department, Japan Marine Science and Technology Center, Yokosuka 237-0061, Japan.
hirono@jamstec.go.jp

Initial receipt: 9 October 2001
Acceptance: 2 June 2003
Web publication: 25 August 2003
Ms 185SR-002

PERMEABILITY MEASUREMENT

During Leg 185, five whole-round samples and eight pieces of representative sediments and rocks from Site 1149 were taken and immediately sealed in bags for subsequent shore-based permeability experiments. Rock pieces were cut into a cylindrical shape for the measurement. Images of the samples are shown in Figure **F1.** Using the fragments of sediments and rocks, wet bulk density, porosity, void ratio, water content, and electrical resistivity were measured (Table **T1**).

Before the permeability testing, the samples should be consolidated under the estimated in situ confining pressure. The estimation is based on the following equation:

Vertical stress = (density of upper material – density of seawater) x depth below seafloor x gravitational acceleration.

Because clayey samples often show intense dilatancy after coring, it is necessary to perform a consolidation test under the estimated confining pressure. The pressures are 0.74 kgf/cm^2 for Section 185-1149A-3H-4; 2.72 kgf/cm^2 for Section 8H-4; 4.54 kgf/cm^2 for Section 13H-4; 5.80 kgf/cm^2 for Section 17H-2; and 6.56 kgf/cm^2 for Section 3R-1. Hard rocks have slight dilatancy, so the confining pressure of 5.00 kgf/cm^2 was used for all the rocks. The triaxial compressive machine was used for testing the samples (Fig. **F2**). The consolidated volumes are plotted with time (Fig. **F3**). The volume of clayey samples decreases with time, and pelagic clays show secondary consolidation that may result from rearrangement of clay minerals. After this testing, permeabilities were measured under the confined pressure and room temperature (20°C). The experiments were conducted by the steady-state method, which entails measurement of volumetric flow-through rate under a constant fluid pressure gradient. The measurements have good linearities between the volume of outflow and time. Measured permeabilities are shown in Table **T1.**

IONIC DIFFUSIVITY MEASUREMENT

The elementary processes of mass transport in geomaterial are not only advection but also diffusion. Diffusion describes the mass transfer process due to the random thermal motion of molecules, ions, and atoms (also known as Brownian motion), which is represented by a molecular random walk. Diffusion causes mass flux down a concentration gradient and results in the spreading of a concentration front with time toward the random distribution of molecules for increasing entropy. The mass flux per unit cross-sectional area depends on the concentration gradient, known as Fick's first and second laws (Fick, 1855) and is expressed as follows:

$$F = D\delta C/\delta x, \text{ and}$$

$$\delta C/\delta t = D\delta^2/\delta x^2,$$

where D is the diffusion coefficient and $\delta C/\delta x$ is the concentration gradient.

Trough diffusion experiments were used for the measurement of effective diffusion coefficients (Fig. **F4A**). Rock samples were fitted tightly

F1. Core samples, p. 6.

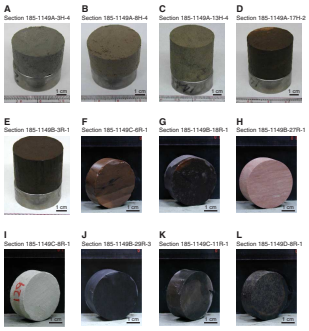

T1. Moisture and density, permeability, and diffusivity, p. 14.

F2. Triaxial compression instrument, p. 7.

F3. Consolidated volume vs. time, p. 8.

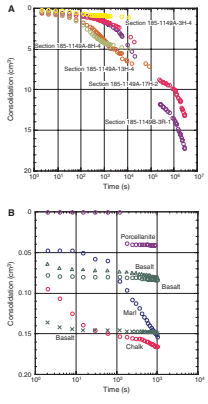

F4. Calculation of effective diffusion coefficient, p. 9.

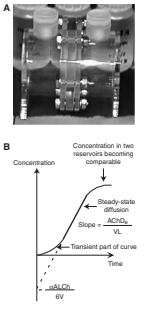

into the central support member of the cell, and the space between the rock disk and the acrylic central support member was sealed with a silicone gasket. There are two cells on both sides of the sample, one for a tracer and another for pure water. Samples were soaked in pure water under vacuum for 1 week to evacuate all air from the interconnected pores. The experiments were conducted under the following conditions: 25°C temperature and atmospheric pressure. Potassium iodine solution (concentration = 1 mol/L) was used as a tracer because the iodine ion is generally not adsorbed on the surface of the rock matrix.

The solution of Fick's second law (Crank, 1975) under an initial condition of

$$C(x,0) = 0$$

for

$$0 \le x \le 1$$

and boundary conditions of

$$C(0,t) = C_1 \text{ and}$$

$$C(x,t) = C_2 = 0 \ (<<C1)$$

is expressed as:

$$C_2(t) = \frac{ALC_1}{V_2}\left\{\frac{D_e t}{L^2} - \frac{\alpha}{6} - \frac{2\alpha}{\pi^2}\sum_{n=1}^{\infty}\frac{(-1)^n}{n^2}\exp\left(-\frac{D_e n^2 \pi^2 t}{L^2 \alpha}\right)\right\}$$

where

C_1 = concentration of the ion in the tracer vessel,
V_1 = vessel volume,
C_2 = concentration of the ion in the pure water vessel,
V_2 = vessel volume,
A = cross-sectional area of the specimen, and
L = sample thickness.
α = rock capacity factor.

The above diffusion equation approaches for a sufficient long time, t, the following expression for the concentration in the pure water vessel:

$$C_2(t) = \frac{ALC_1}{V_2}\left(\frac{D_e t}{L^2} - \frac{\alpha}{6}\right)$$

At this time, this diffusion process can be treated as a steady state and the effective diffusion coefficient can be calculated by the line slope of ion concentration with time (Fig. F4B). Iodine and potassium ions were measured by an ion-selective electrode and atomic absorption spectrometry, respectively.

The concentrations of iodine and potassium ions during the diffusion experiments are plotted as a function of time (Figs. F5, F6). All the plots indicate that the concentrations increase with time, showing a transient part and a steady-state slope. As mentioned above, the effective diffusion coefficient is calculated by the linear slope of the data.

F5. Ion concentrations in clayey sediments, marl, and chalk, p. 10.

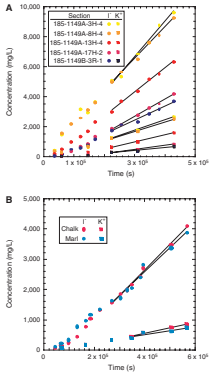

F6. Ion concentrations in porcellanite, chert, and basalts, p. 11.

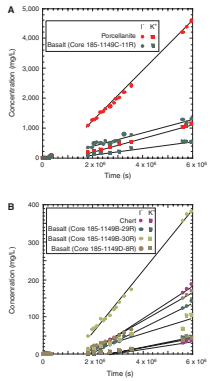

The effective diffusion coefficient can be calculated using the slope, geometry, and volume of the cell (Table T1).

PERMEABILITY-DEPTH PROFILE

Log permeability and log diffusivity were shown vs. the porosity (Fig. F7) In the log permeability and porosity plot, two trends can be recognized (Fig. F7A): one for clay and one for hard rocks. Assuming parallel-sided or sphere-shaped pores, permeability is linear to the third power of porosity (Gueguen and Palciauskas, 1994). Poiseuill flow in cylindrical tubes leads to the relationship that permeability is linear with the square of porosity (Gueguen and Palciauskas, 1994). The fitting third-power law assumed between permeability and porosity of chalk, marl, chert, porcellanite, and basalt indicates the following relation:

$$k = 1.2 \times 10^{-15} \times \phi^3,$$

where k is permeability and ϕ is porosity. In the clayey samples, there is no suitable second- or third-power law for fitting the equation. The best-fit equation is as follows:

$$k = 1.4 \times 10^{-33} \times \phi^{12.87}.$$

Based on both the power law of permeability-porosity relationship and porosity-depth profile, the downhole-scale permeability profile can be reconstructed (Fig. F8). Porosities were measured using discrete samples or downhole logging (Accelerator Porosity Sonde [APS]). Because there was no porosity data in pelagic clay between 150 and 180 meters below seafloor (mbsf), permeability shows value are constant.

ACKNOWLEDGMENTS

This research used samples and/or data provided by the Ocean Drilling Program (ODP). ODP is sponsored by the U.S. National Science Foundation (NSF) and participating countries under management of Joint Oceanographic Institutions (JOI), Inc. Funding for this research was provided by Research Fellowships of the Japan Society for the Promotion of Science for Young Scientists.

F7. Permeability, porosity, and effective diffusion coefficients, p. 12.

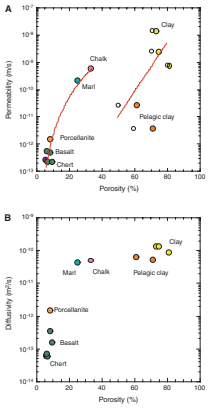

F8. Permeability profile, p. 13.

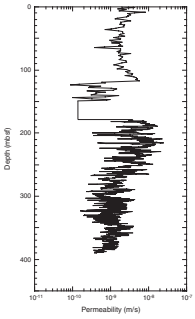

REFERENCES

Armstrong, R.L., 1968. A model for Sr and Pb isotopic evolution in a dynamic Earth. *Rev. Geophys.,* 6:175–191.

Crank, J., 1975. *The Mathematics of Diffusion:* Oxford (Oxford Univ. Press).

Fick, A., 1855. On liquid diffusion. *Philos. Mag.,* 294:30–39.

Gueguen, Y., and Palciauskas, V., 1994. *Introduction to the Physics of Rocks:* Princeton (Princeton Univ. Press).

Karig, D.E., and Kay, R.W., 1981. Fate of sediments on the descending plate at convergent margins. *Philos. Trans. R. Soc. London,* 301:233–251.

Plank, T., and Langmuir, C.H., 1993. Tracing trace elements from sediment input to volcanic output at subduction zones. *Nature,* 362:739–743.

von Huene, R., and Scholl, D.W., 1991. Observations at convergent margins concerning sediment subduction, subduction erosion, and the growth of the continental crust. *Rev. Geophys.,* 29:279–316.

Figure F1. Core samples from the subducted oceanic plate around the Mariana-Izu Trench drilled during Leg 185. **A, B, C.** Silty clays. **D, E.** Pelagic clays. **F.** Porcellanite. **G.** Chert. **H.** Chalk. **I.** Marl. **J, K, L.** Basalts.

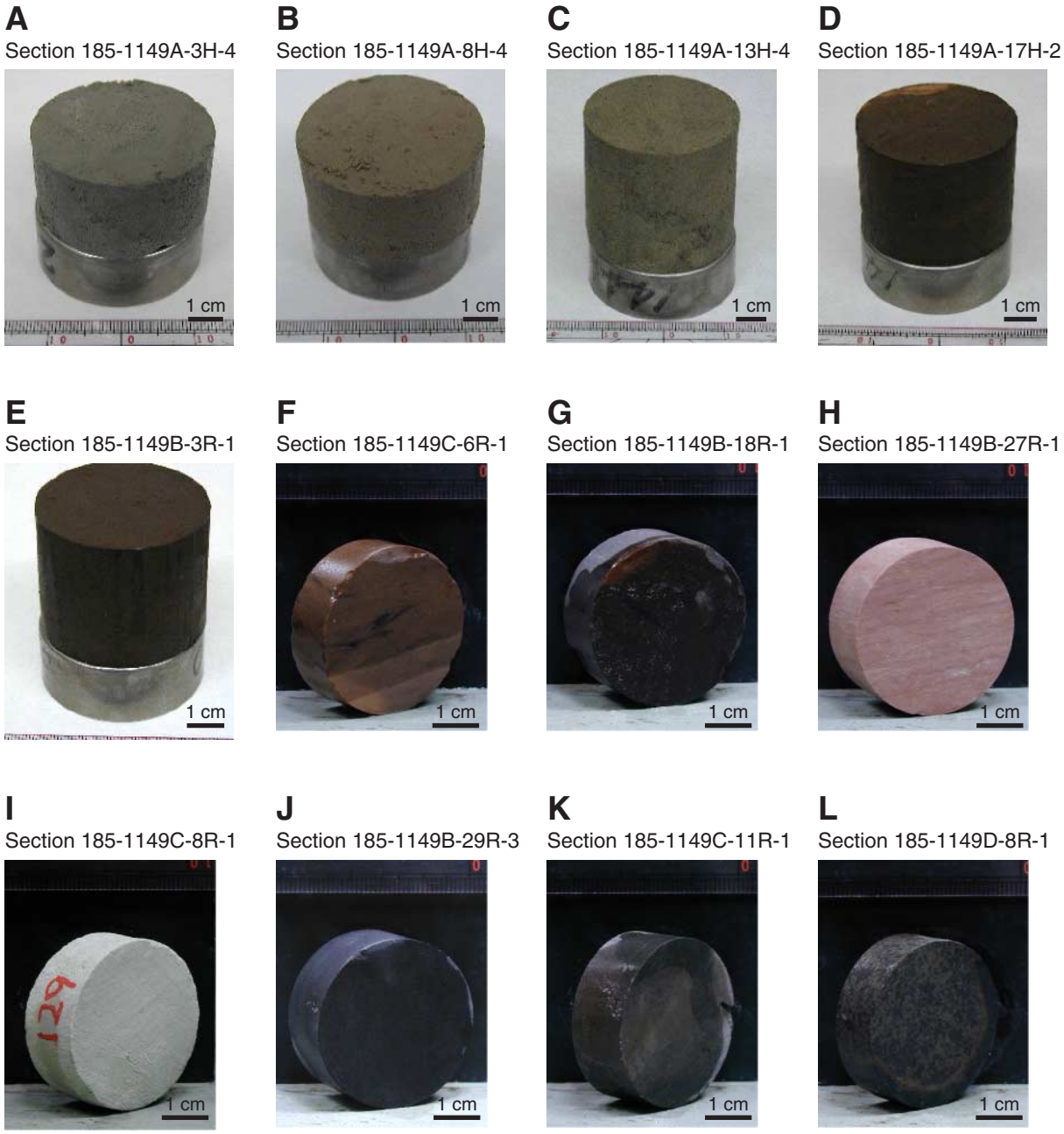

Figure F2. Triaxial compression instrument for consolidation and permeability testing.

Figure F3. Plots for consolidated volume with time. **A.** Clayey sediments. **B.** Hard rocks.

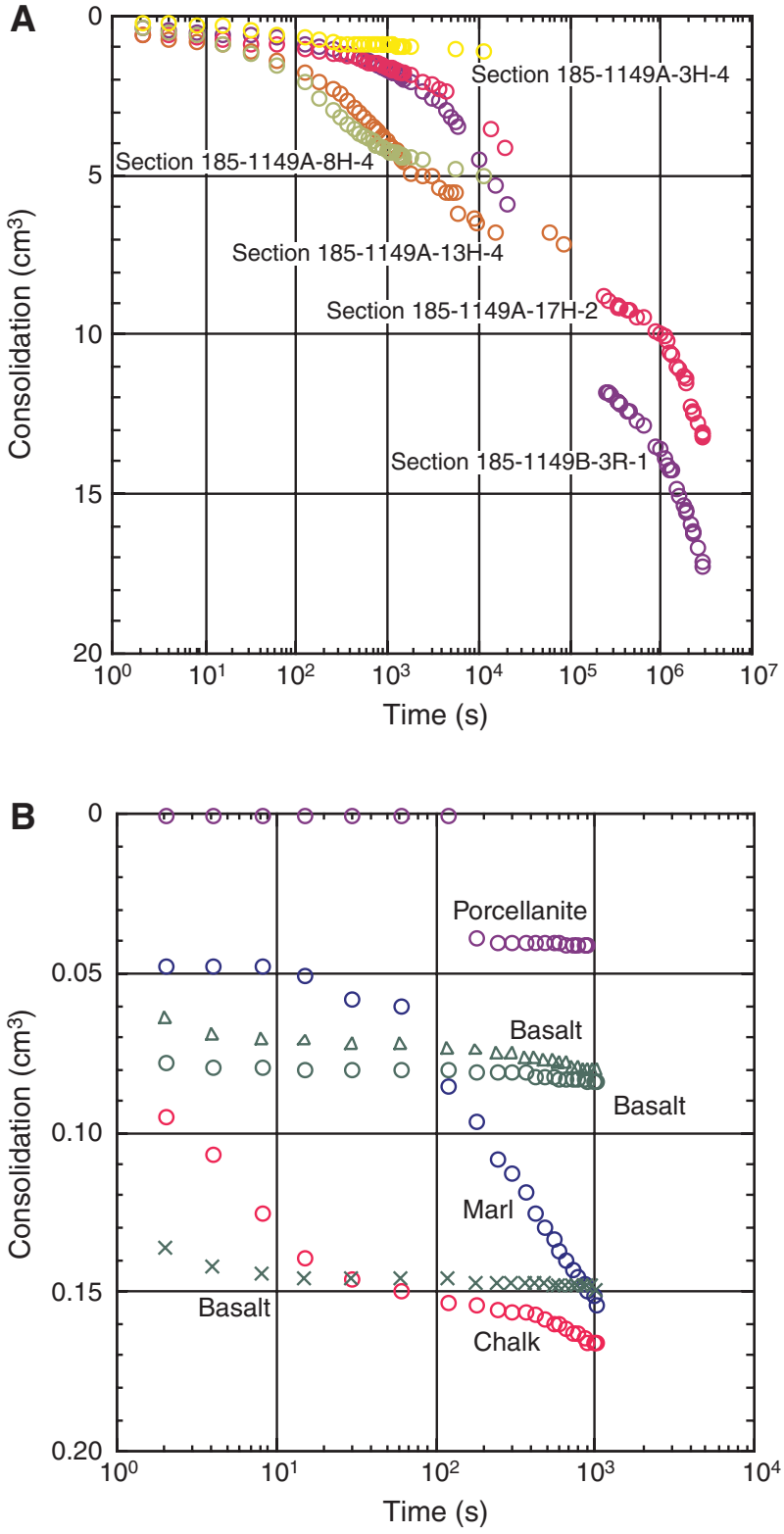

Figure F4. A. Vessels for through-diffusion testing. **B.** Calculation of the effective diffusion coefficient. See "Ionic Diffusivity Measurement," p. 2, for definitions of equation variables.

A

B

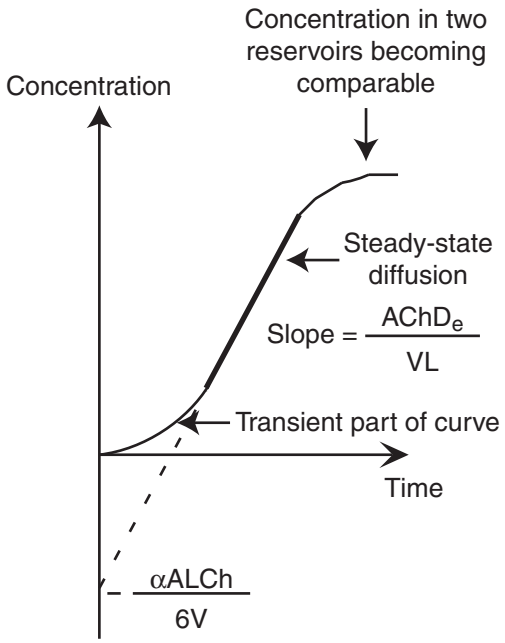

Figure F5. Plots for ion concentration and time. **A.** Clayey sediments. **B.** Marl and chalk.

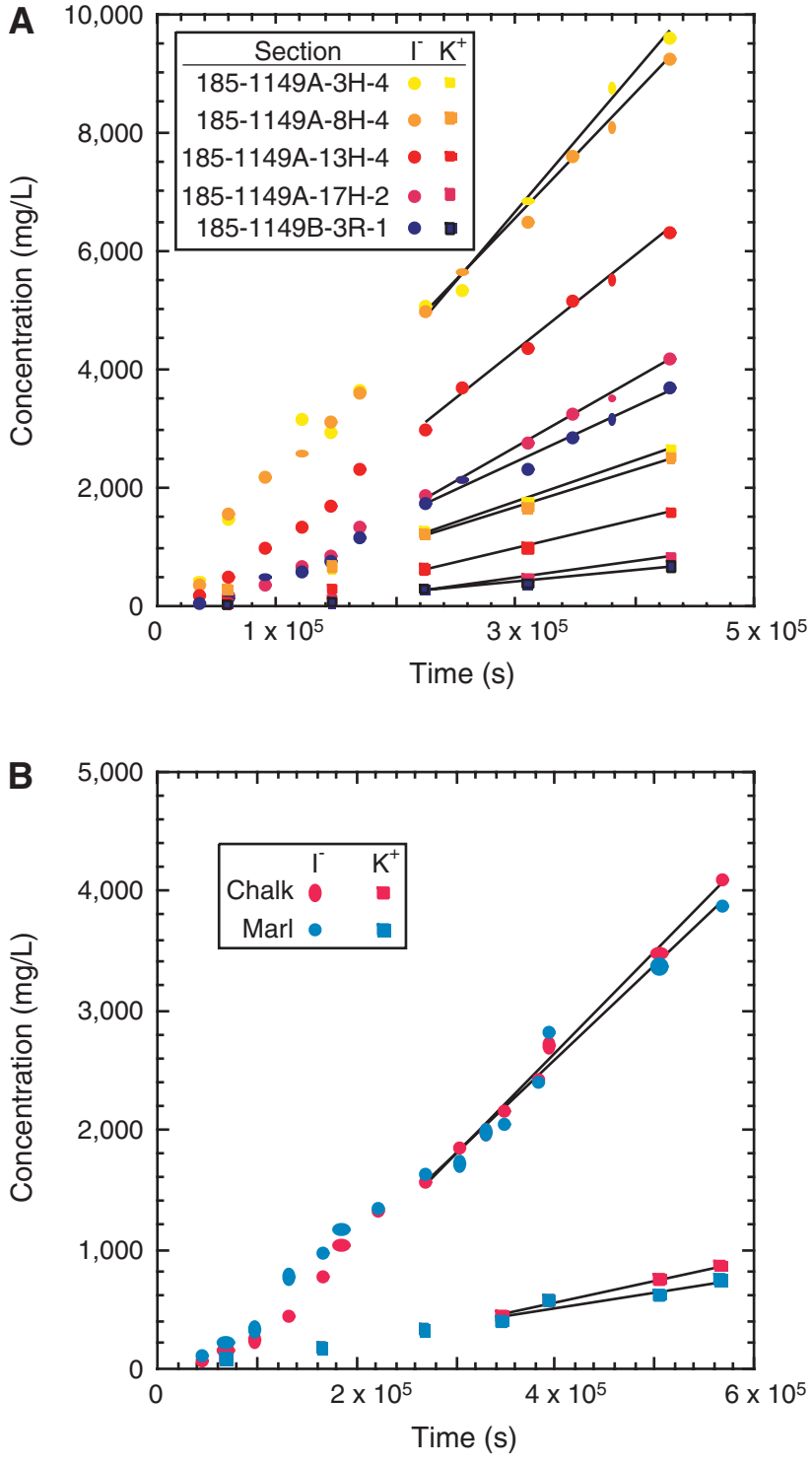

Figure F6. Plots for ion concentration and time. **A.** Porcellanite and basalt. **B.** Chert and basalts.

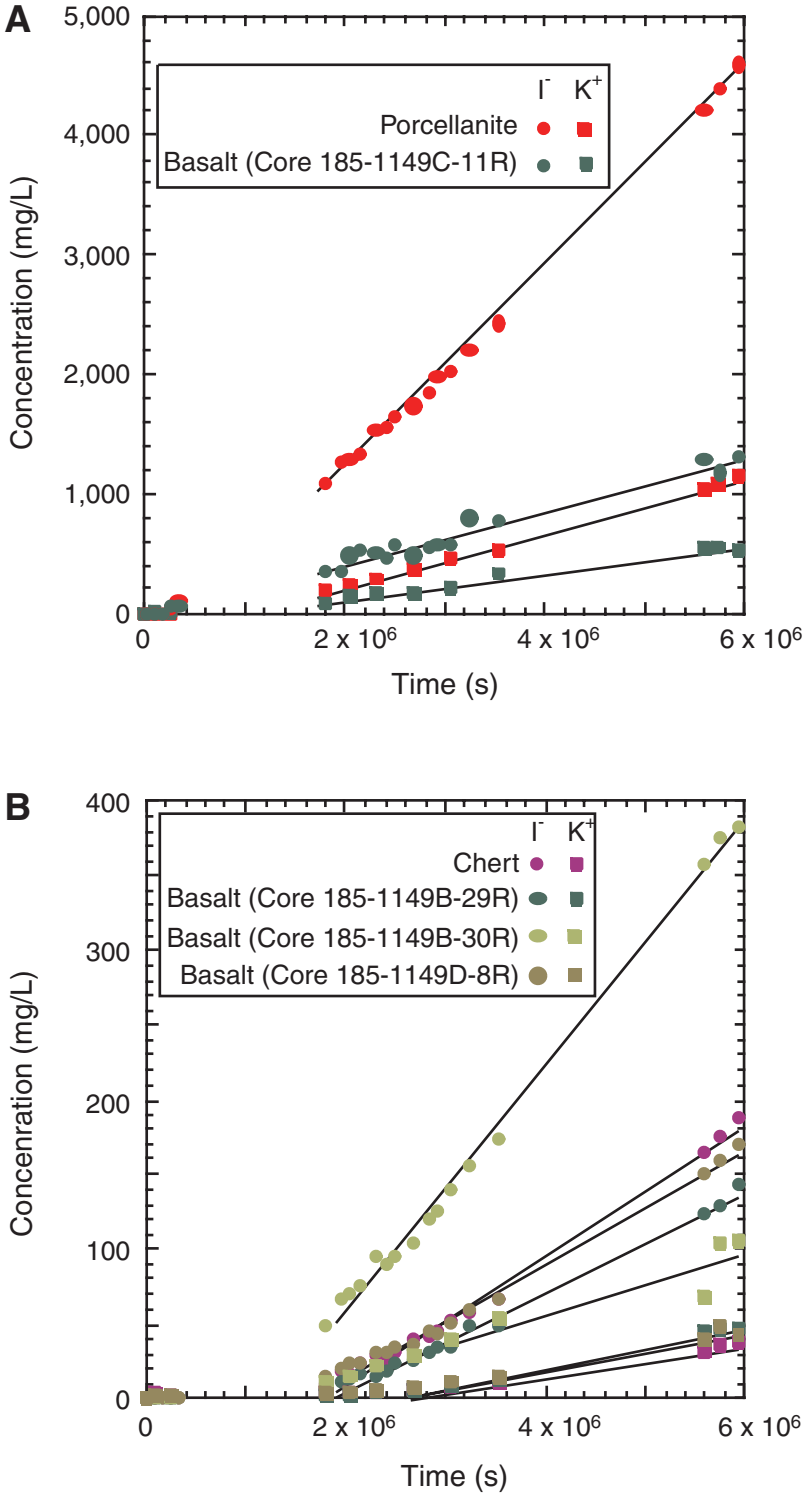

Figure F7. A. Plots for permeability and porosity. **B.** Plots for effective diffusion coefficient of iodine ion and porosity.

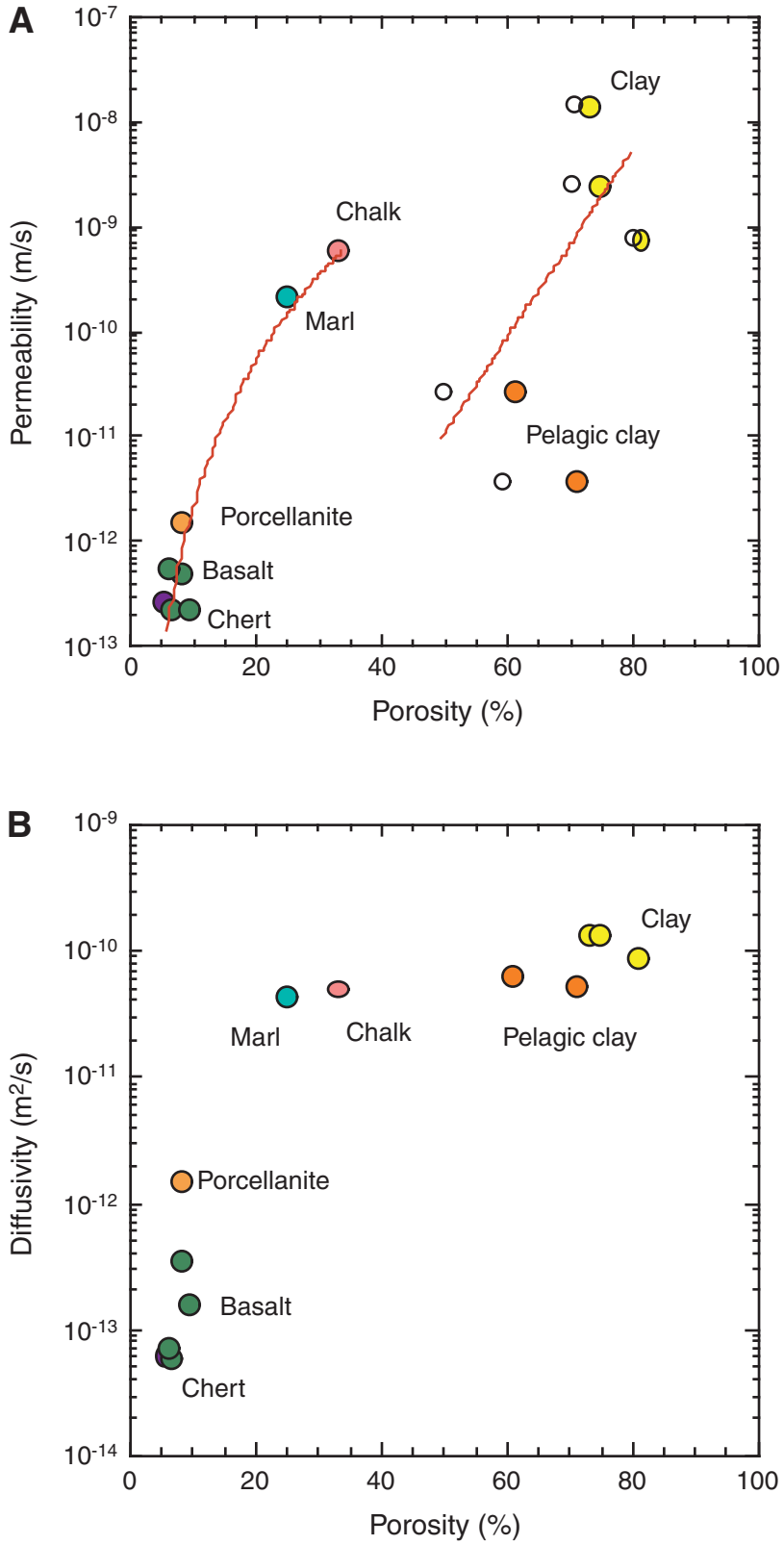

Figure F8. Permeability and depth profile.

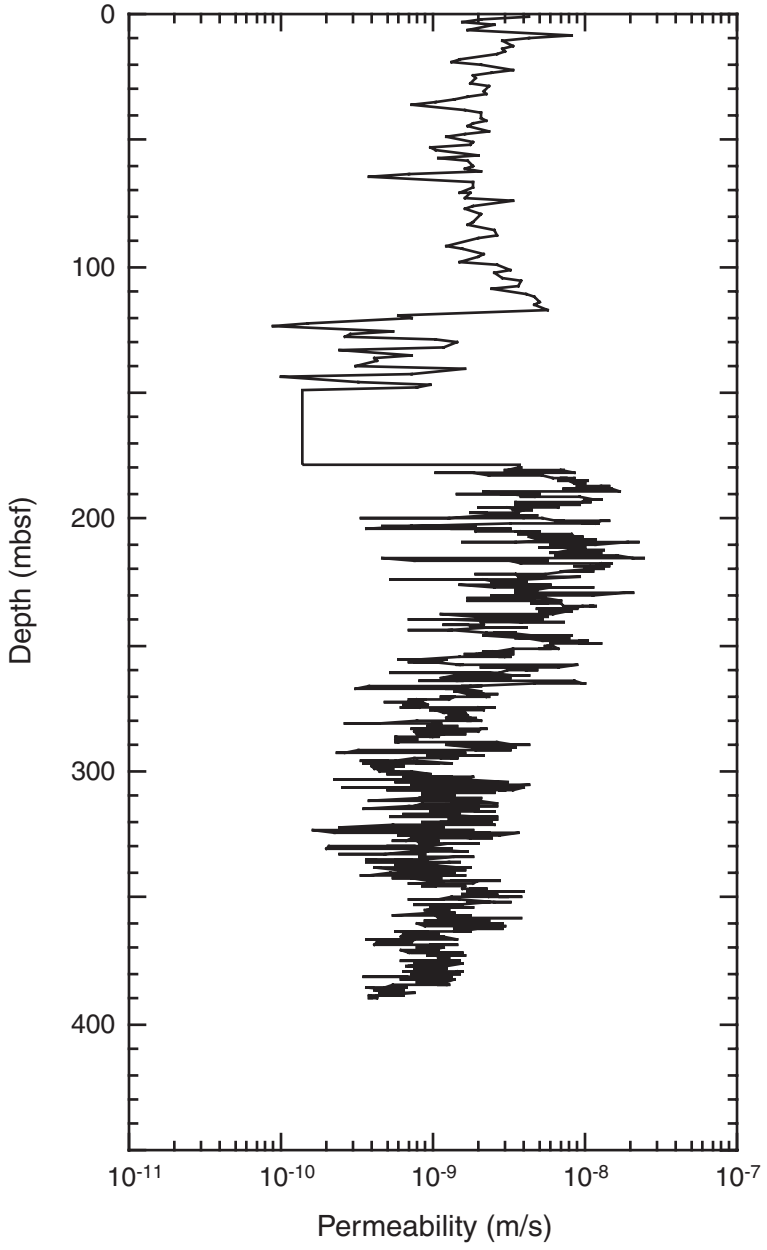

Table T1. Moisture and density, permeability, and diffusivity, Site 1149.

Core, section	Depth (mbsf)	Lithology	Wet bulk density (g/cm^3)	Porosity (%)	Void ratio	Water content (%)	Resistivity (Ωm)	Permeability (m/s)	I^- diffusivity (m^2/s)	K^+ diffusivity (m^2/s)	*P*-wave velocity (m/s)	CT value
185-1149A-												
3H-4	19.50	Clay	1.46	72.9	2.69	51.2	68.65	1.44E–08	1.38E–10	1.35E–10	1532	696
8H-4	67.10	Clay	1.43	74.8	2.97	53.5	73.83	2.52E–09	1.37E–10	1.21E–10	1515	832
13H-4	114.60	Clay	1.33	80.9	4.24	62.5	33.66	7.51E–10	9.10E–11	8.75E–11	1554	640
17H-2	149.60	Pelagic clay	1.36	60.8	1.55	45.7	32.2	2.73E–11	6.25E–11	4.77E–11	1522	944
185-1149B-												
3R-1	171.70	Pelagic clay	1.50	70.8	2.43	48.5	49.68	3.72E–12	5.37E–11	3.79E–11	1508	1328
18R-1	302.81	Chert	2.33	5.1	0.05	2.2	3665.33	2.75E–13	6.12E–14	4.05E–14	4946	2000
27R-1	387.60	Chalk	2.21	32.9	0.49	15.2	80.47	6.09E–10	4.94E–11	3.24E–11	2172	2016
29R-3	410.58	Basalt	2.69	6.4	0.07	2.5	632.7	2.25E–13	5.97E–14	6.55E–14	4606	2781
30R-2	418.33	Basalt	2.59	9.0	0.10	3.5	355.93	2.24E–13	1.58E–13	1.30E–13	4840	2641
185-1149C-												
6R-1	312.87	Porcellanite	2.19	8.0	0.09	3.7	3491.46	1.55E–12	1.52E–12	1.41E–12	3219	1797
8R-1	388.67	Marl	2.37	24.7	0.33	10.7	135.65	2.17E–10	4.48E–11	2.53E–11	2356	1828
11R-1	418.41	Basalt	2.31	8.1	0.09	3.6	459.77	5.13E–13	3.52E–13	5.71E–13	5167	2016
185-1149D-												
8R-1	330.13	Basalt	2.77	5.9	0.06	2.2	427.46	5.64E–13	7.01E–14	6.59E–14	4569	1828

Notes: CT = X-ray computed tomography. CT value of air = –1000. Water = 0.